Shock Front Width and Structure in Supersonic Granular Flows

J. F. Boudet, Y. Amarouchene, and H. Kellay
Université Bordeaux1, Centre de Physique Moléculaire Optique et Hertzienne, UMR 5798 du CNRS, 351 cours de la Libération, 33405 Talence, France
(Received 22 May 2008; published 19 December 2008)

The full structure of a shock front around a blunt body in a quasi-two-dimensional granular flow is studied. Two features, a large density gradient and a very small thickness of the front, characterize this shock and make it different from shocks in molecular gases. Both of these features can be understood using a modified version of the granular kinetic theory. Our model separates the particles into two subpopulations: fast particles having experienced no collisions and randomly moving particles. This separation is motivated by direct measurements of the particle velocities which show a bimodal distribution. Our results not only shed new light on the use of the granular kinetic theory under extreme conditions (shock formation) but bring new insight into the physics of shocks in general.

DOI: 10.1103/PhysRevLett.101.254503 PACS numbers: 47.40.Ki, 47.45.Ab, 47.57.Gc

Fluid flow around an obstacle has been a paradigm for testing theories of simple and complex fluid flows. The role of viscous stresses, the different instabilities that arise, the transition to turbulence, the formation of shock waves, are examples of the rich phenomenology of such a situation. A granular material flowing around an obstacle engenders yet another even more complex phenomenology. Previous observations have shown the existence of shock waves [1–3], the formation of patterns [4], as well as a complex dependence of the drag force versus velocity and density [5–8]. While of utmost importance for understanding flows in liquids, the issue for a granular material flowing around an obstacle is still not completely understood. For instance, the formation of shocks can be readily observed in dilute granular flows around an obstacle. The properties of these shocks can be understood using continuum equations derived from the granular kinetic theory [1]. The speed of sound and its variation with density can also be understood using arguments from this theory [2]. For higher densities, the shock front develops very steep density gradients, however, [4] and kinetic theory may break down as large clusters form around the obstacle. Dense clusters are routinely reported in experiments and simulations of driven granular media [9–12]. Here, we examine, experimentally, the flow region near the obstacle for a supersonic quasi-two-dimensional granular flow at varying volume fractions. The details of this situation reveal several features such as a gradual transition from gas to liquid to solid in the vicinity of the obstacle. The dense region is separated from the incident stream by a well-defined interface. This shock front has a width and a structure which can be understood using a simple model.

Our setup consists of two parallel glass plates set vertically and spaced by a distance h of a few particle diameters so our set up is quasi-two-dimensional. A circular obstacle with a radius R and thickness h is inserted between the plates. The summit of the obstacle is placed at distances between 11 and 25 cm from the entrance of the cell. Glass beads (diameter $d = 0.5$ mm) or steel spheres ($d = 2$ mm) are then poured in the spacing between the plates from a reservoir equipped with a gate whose opening controls the injection flux. Four different values of the ratio h/d are used: 2, 4, 6, and 8. The flow of these grains in the cell, which fall under the action of gravity, is filmed using a fast camera working at 4000 frames/s from which the particle field and the velocity field can be obtained using a particle tracking technique or particle imaging velocimetry. Laser Doppler velocimetry (LDV) is used to measure the horizontal (x) and vertical (z) velocity components and their temporal fluctuations for the glass beads [13,14] at a single location. This ensemble of measurements allows for an accurate determination of the spatial variation of the mean density as well as the spatial variation of the mean velocity and its standard deviation. Since imaging of the cell gives the time averaged surface fraction of particles ϕ_s in the cell, we convert ϕ_s into a volume fraction using a direct calibration and computer simulations. It turns out that the time averaged volume fraction ϕ_V can be obtained reliably from measurements of the surface fraction for thicknesses up to a few grain diameters with the result $\phi_V = \frac{2}{3}(1 - (1 - \phi_s)^{d/h})$.

The interaction of the flow with the obstacle is illustrated in Fig. 1. When only a few grains fall, they interact solely with the obstacle. As the number of grains increases, the grains not only hit the obstacle but start colliding with each other and with the incoming stream giving rise to a large number of collisions in the region near the obstacle. As the volume fraction of the incident flow ϕ_∞ increases, the region on top of the obstacle is host to an important accumulation of grains with local volume fractions close to a typical random loose packing value. This occurs for a value of ϕ_∞ which decreases with the radius of the obstacle and which can be as small as 0.014. Note that the height of the dense region increases as ϕ_∞ increases (and

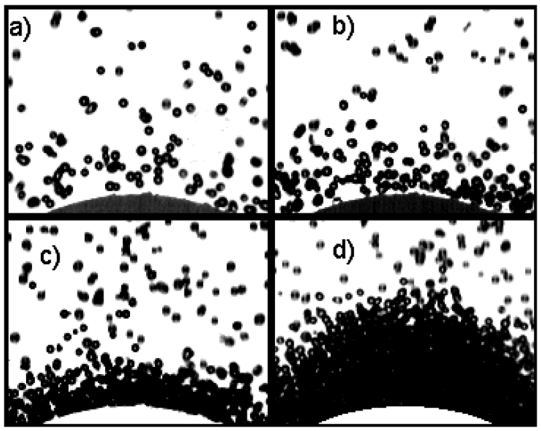

FIG. 1. Photographs of the flow around a cylinder ($R = 12$ mm, $h = 2$ mm, glass beads of $d = 0.5$ mm) for different $\phi_\infty = 0.004$, 0.006, 0.01, and 0.017.

as R increases). To appreciate this point, we plot, in Fig. 2, the time averaged local volume fraction $\phi_V(z)$ along a vertical cut. The origin of the vertical z axis is the summit of the cylinder. The bottom inset of Fig. 2 shows the linearity between an imposed ϕ_V and the volume fraction obtained from a measurement of ϕ_s using the expression quoted above which validates our conversion. Figure 2 illustrates that for very low ϕ_∞, the volume fraction starts out at the injection value far from the obstacle and increases as the obstacle is approached. As ϕ_∞ increases, the maximum of the volume fraction $\phi_v^{\max}$ near the obstacle

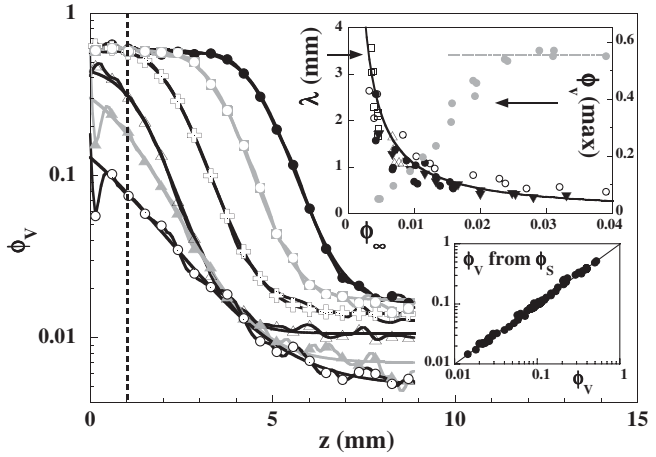

FIG. 2. $\phi_V(z)$ for increasing ϕ_∞: 0.005, 0.007, 0.01, 0.014, 0.015, and 0.017. $R = 12$ mm, $h = 2$ mm, and glass beads. The lines are fits to a hyperbolic tangent profile. The vertical line indicates the position of the measurements of Fig. 4. Upper inset: characteristic length λ of the density profiles for glass beads (squares and triangles: 6 mm $\leq R \leq$ 27 mm, $h = 4$ mm, and $\phi_\infty = 0.0045$ and 0.007, respectively, filled triangle: $R = 6$ cm and $h = 2$ mm, circles: $R = 6$ mm and $h = 4$ mm, filled circles: $R = 12$ mm and $h = 2$ mm) and maximal density $\phi_V^{\max}$ versus ϕ_∞ ($R = 6$ mm, $h = 2$ mm). Lower inset: ϕ_V deduced from ϕ_s versus the imposed ϕ_V. Data obtained using different thicknesses $h = 2d$ for steel spheres and $h = 4d$ for glass beads.

increases gradually versus ϕ_∞ as shown in the inset of Fig. 2. Beyond ϕ_∞ of about 0.02, $\phi_V^{\max}$ saturates at a value close to the random loose packing value indicated by a dotted line. In addition to the gradual increase of $\phi_V^{\max}$, the shape of $\phi_V(z)$ varies. This variation can be parametrized using a hyperbolic tangent profile with a characteristic length scale 2λ. The inset of Fig. 2 displays the scale λ which is large for low ϕ_∞ and decreases as ϕ_∞ increases. Note that λ starts out near 4 mm (8 grain diameters) and decreases rapidly to reach values near one grain diameter at ϕ_∞ near 0.015. At higher ϕ_∞, $\phi_V(z)$ does not change markedly as shown in Fig. 2. The decay length is the same while the position of the interface shifts to higher z values. The conclusion from the measurements of Fig. 2 is that the grains accumulate on top of the obstacle to form a dense phase whose density increases gradually and whose interface with the gaseous phase (the injected stream) becomes sharper as ϕ_∞ increases. This dense phase is the result of the collisions of the grains with the obstacle and the injected stream. The presence of a density gradient is characteristic of a shock front and Fig. 2 therefore shows its full structure with its very high density gradient and its very sharp interface. The shock thickness, given by 2λ, is only a fraction of the mean free path $l(\phi_\infty) = \frac{d}{6\sqrt{2}\phi_\infty}$. The solid line in the upper inset of Fig. 2 is given by $\frac{l(\phi_\infty)}{6}$ and is independent of the ratios h/d used here and the radius R. In contrast, the shock wave thickness in molecular gases at high Mach numbers is roughly four mean free paths [15–17]. Using the same definition as for shocks in gases, the equivalent thickness here is $\frac{4l(\phi_\infty)}{6}$.

To complement these density measurements we have measured the velocity field and the velocity fluctuations versus ϕ_∞. An example of such a measurement showing the time averaged velocity field $\langle \mathbf{V} \rangle$ as well as the standard deviation of the velocity fluctuations $1/2(\delta V_z^2 + \delta V_x^2)$, related to an effective granular temperature $T \sim \delta \mathbf{V}^2$ (the component V_y was not measured), is presented in Fig. 3. While the streamlines are vertical in the upstream part of the flow, they curve near the interface and the velocity decreases as the obstacle is approached. The velocity standard deviation is low in the upstream region, increases near the interface and decreases as the summit of the obstacle is reached. While the velocity decrease and the rise in velocity fluctuations are expected for a shock front in molecular gases [17], the cooling is not. To illustrate the cooling which accompanies the density increase near the obstacle, we fix the position of the velocity measurements at 1 mm from the summit and vary ϕ_∞. The experimental conditions correspond to those of Fig. 2. Figure 4 shows that the probability density functions (PDF) of V_x and V_z (obtained from LDV measurements) are similar indicating a relatively isotropic state of agitation near the obstacle. The shape of the PDFs is very different from a Gaussian. Note that as ϕ_∞ increases a sharp transition to much narrower PDFs occurs: a small variation of the injection volume fraction leads to a large reduction of the width of the

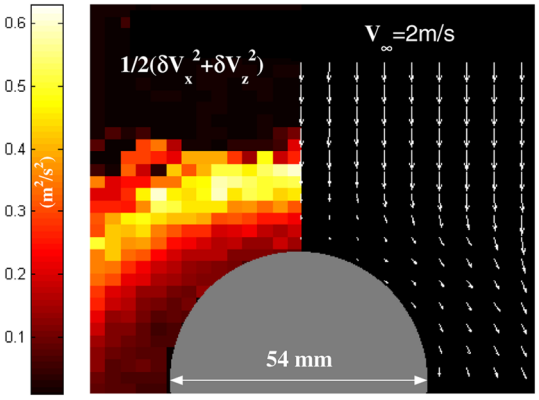

FIG. 3 (color online). Velocity standard deviation and velocity field for steel spheres ($R = 27$ mm and $h = 4$ mm).

velocity PDFs. The measurement of the velocity standard deviation as well as the local density are shown in the inset. While the fluctuations in velocity are high for low densities, they decrease rapidly as the density increases. A cooling of the granular medium is therefore observed indicating a transition from gas to liquid and probably to a solid like phase as ϕ_∞ increases. This decrease in the granular temperature of the dense zone is also observed in a series of experiments where ϕ_∞ is fixed and the distance z is varied. This feature can be appreciated from a plot of the PDFs of the vertical velocity V_z as shown in Fig. 5. While far from the obstacle the PDF has a single peak at the incident stream velocity V_∞, as the obstacle is approached from above, the PDF becomes bimodal with a peak at V_∞ and a peak centered at zero. Collisions with other particles are important in giving rise to the peak at zero. As z decreases, the peak at V_∞ decreases in height at the expense of the peak at zero. Well inside the dense region, the peak at nonzero velocity disappears completely and the width of the PDF starts to decrease showing the cooling discussed above. One can therefore distinguish two subpopulations of particles: the fast particles and the randomly flying slower ones. This feature is observed for the different values of h/d used here, and obtained using both LDV and particle tracking velocimetry, and for regions where the local volume fraction is sufficiently small to rule out effects due to the presence of the walls such as local crystallization, for example.

In gases, the shock thickness decreases as the Mach number M increases and saturates for large M (>5) at about 4 times the mean free path of the gas molecules [15,17]. In our case, the Mach number is about 9 for the glass beads [2] and about 20 for the steel spheres [1] and while the thickness λ varies versus density it remains proportional to but much smaller than the mean free path (see Fig. 2). This fact as well as the structure of the shock wave with its very large density gradient can be understood using a simple one dimensional model. The model uses elements of granular kinetic theory [18–21]with additional input. The main ingredient of our model is that the population of particles can be separated into two subpopulations. The first subpopulation is composed of particles that have experienced no collisions and fall with a velocity V_∞ and a volume fraction $f(z)\phi_\infty$. The function $f(z)$ starts at a value of 1 far from the obstacle, decreases near the interfacial region and goes to zero very near the obstacle. The second population is composed of particles that have experienced at least one collision and whose mean velocity will be noted $\mathbf{V}^*$, volume fraction ϕ^* (which is small far from the obstacle and increases as the obstacle is approached), and granular temperature T^*. This separation is inspired by the results of Fig. 5 which show that the vertical velocity is bimodal. The volume fractions of the two subpopulations are related by the conservation of the mass flux which reads $\phi^* V_z^* + f(z)\phi_\infty V_\infty = \phi_\infty V_\infty$. The

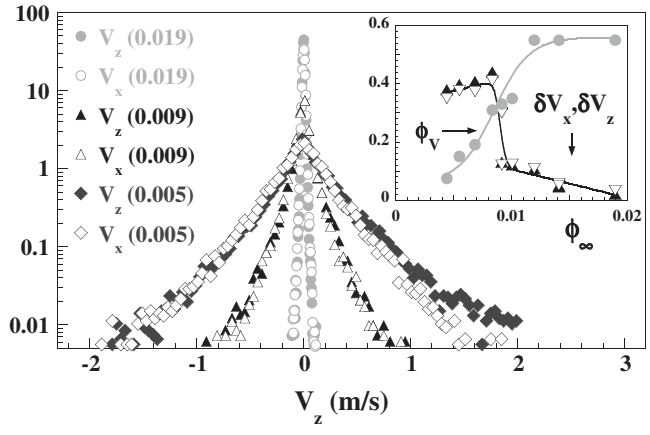

FIG. 4. PDFs of V_z and V_x for a fixed position from the cylinder (1 mm) and varying ϕ_∞ given in parentheses. Inset: δV_z (m/s) (filled triangles), δV_x (m/s) (open triangles), and ϕ_V versus ϕ_∞. ($R = 12$ mm, $h = 2$ mm, glass beads).

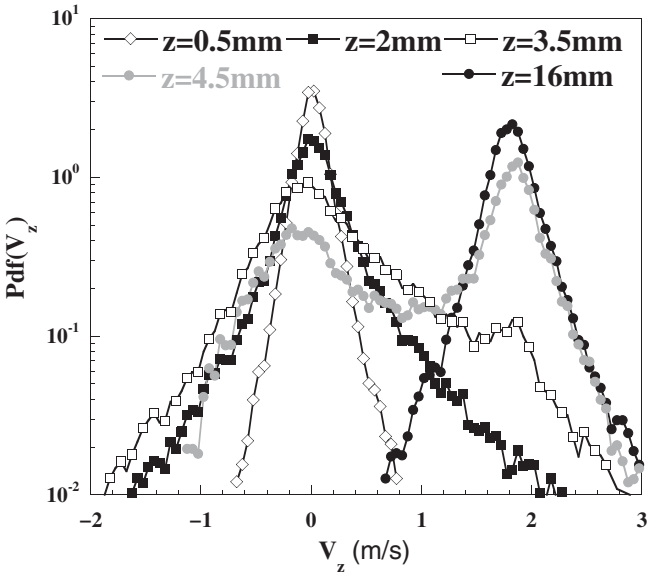

FIG. 5. PDFs of the velocity V_z for a fixed $\phi_\infty = 0.016$ and varying positions z (glass beads, $R = 12$ mm, $h = 2$ mm).

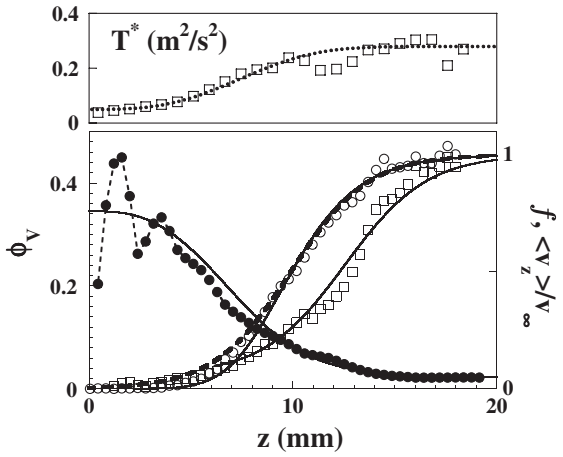

FIG. 6. Volume fraction (solid circles), temperature, velocity (squares), and $f(z)$ (open circles) along with the calculated variations from our model (solid lines). The dashed line is a fit of $f(z)$ using the expression in the text. (Steel spheres, $R = 27$ mm, $h = 4$ mm, $\phi_\infty = 0.022$, $V_\infty = 2.1$ m/s).

momentum balance equation reads: $\frac{d}{dz}(P^* + \phi^* V_z^{*2}) = -\frac{df(z+d)}{dz}\phi_\infty V_\infty^2$. The pressure P^* is taken as $\phi^* T^*(1 + \phi^*/\phi_c)/(1 - \phi^*/\phi_c)$ [10,12]with ϕ_c the random close packing volume fraction. The quantity $f(z)$ is measured experimentally by thresholding the particle velocity V_z obtained from particle tracking to distinguish between particles with a velocity close to V_∞ and the rest. The granular temperature is given by $T^*(z) = 1/3(\delta V_z^{*2} + \delta V_x^{*2} + \delta V_y^{*2})$ and is plotted in Fig. 6. While the standard deviation along z and x are known, that along the direction perpendicular to the plates (y) is not and we assume it is equal to that along x. Note that δV_z^{*2} and δV_x^{*2} are similar in the dense region as we have observed before (Fig. 4) but differ slightly farther out. Also, both quantities present a plateau in the dilute region and decrease as the obstacle is approached giving rise to the observed variation $T^*(z)$. We define a local mean free path $l(\phi^*)$ as follows: $d/(6\sqrt{2}\phi^*)$. An additional ansatz concerns the variation of $f(z)$ which we take as $df(z)/dz = f/l(\phi^*)$ which states that the fraction of fast particles changes over a length scale given by the locally defined mean free path in agreement with our experimental data. By using the measured $T^*(z)$, a value of $\phi_c = 0.54$ (smaller than the random close packing fraction but close to the loose packing value) and the proposed variation of $f(z)$, the momentum balance equation can be solved numerically. The results of this calculation are displayed in Fig. 6 where we plot the volume fraction $\phi_V(z) = \phi^* + f\phi_\infty$, the mean velocity $\langle V_z \rangle$, and $f(z)$ along with the results obtained from the numerical solution. The agreement is good for $f(z)$, $\langle V_z \rangle$, and $\phi_V(z)$. The length scale λ coming out of this calculation is similar to the one shown above in Fig. 2: $l(\phi_\infty)/6$. The prefactor can be understood in a simple way. By neglecting dissipation and heat transfer, which is roughly valid in the region where the temperature is constant and the volume fraction small, the energy balance equation [10,22] leads to $f(z) = \{1/[1 + \exp(-(z - z_0)/l'(\phi_\infty))]\}$ with $l'(\phi_\infty) = \lambda = \frac{e^2}{\alpha+2} l(\phi_\infty)$ and z_0 such that $f = \frac{1}{2}$ at $z = z_0$. The value of the restitution coefficient e is 0.93 for steel spheres and 0.85 for glass spheres and $\alpha = 3$ is the number of degrees of freedom per particle. The calculated $f(z)$, which is indistinguishable from the numerical result in Fig. 6, and λ are in excellent agreement with the measured variation.

To summarize, the simple situation of flow around an obstacle for a granular medium is complex giving rise to a shock front whose properties are unlike those of molecular gases. A dense region and large density gradients form around the obstacle. This region grows denser and cooler as the injection flux increases and has a well defined interface with the gaseous region. This interface becomes sharper as the volume fraction increases. The velocity distributions are bimodal with non trivial variations versus density and distance from the obstacle. Several features of this shock front can be understood using a simple one dimensional model based on granular kinetic theory along with a simple ansatz on the separation of the particles into two subpopulations but further theoretical work is needed for a full understanding of shock fronts in granular flows.

[1] E. C. Rericha *et al.*, Phys. Rev. Lett. **88**, 014302 (2001).
[2] Y. Amarouchene and H. Kellay, Phys. Fluids **18**, 031707 (2006).
[3] A. Levy and M. Sayed, Phys. Fluids **19**, 023302 (2007).
[4] Y. Amarouchene, J. F. Boudet, and H. Kellay, Phys. Rev. Lett. **86**, 4286 (2001).
[5] R. Albert *et al.*, Phys. Rev. Lett. **82**, 205 (1999).
[6] C. R. Wassgren *et al.*, Phys. Fluids **15**, 3318 (2003).
[7] D. Chehata, R. Zenit, and C. R. Wassgren, Phys. Fluids **15**, 1622 (2003).
[8] V. Buchholtz and T. Pöschel, Granular Matter **1**, 33 (1998).
[9] A. Kudrolli, M. Wolpert, and J. P. Gollub, Phys. Rev. Lett. **78**, 1383 (1997).
[10] E. L. Grossman, T. Zhou, and E. Ben-Naim, Phys. Rev. E **55**, 4200 (1997).
[11] R. Liu *et al.*, Phys. Rev. E **75**, 061304 (2007).
[12] O. Herbst *et al.*, Phys. Rev. E **70**, 051313 (2004).
[13] J. F. Boudet *et al.*, J. Fluid Mech. **572**, 413 (2007).
[14] H. Kellay, Y. Amarouchene, and J. F. Boudet, Phys. Fluids **19**, 078104 (2007).
[15] M. Linzer and D. F. Hornig, Phys. Fluids **6**, 1661 (1963).
[16] R. E. Center, Phys. Fluids **10**, 1777 (1967).
[17] M. Al-Ghoul and B. C. Eu, Phys. Rev. E **56**, 2981 (1997).M. Al-Ghoul and B. C. Eu, Phys. Rev. E **64**, 046303 (2001).
[18] I. Goldhirsch, Annu. Rev. Fluid Mech. **35**, 267 (2003).
[19] P. K. Haff, J. Fluid Mech. **134**, 401 (1983).
[20] J. T. Jenkins and M. W. Richman, Phys. Fluids **28**, 3485 (1985).
[21] J. T. Jenkins and S. B. Savage, J. Fluid Mech. **130**, 187 (1983).
[22] J. Eggers, Phys. Rev. Lett. **83**, 5322 (1999).